Maximum Correntropy Criterion for Robust Face Recognition

Ran He, *Member*, *IEEE Computer Society*, Wei-Shi Zheng, *Member*, *IEEE Computer Society*, and Bao-Gang Hu, *Senior Member*, *IEEE*

Abstract—In this paper, we present a sparse correntropy framework for computing robust sparse representations of face images for recognition. Compared with the state-of-the-art l^1norm-based sparse representation classifier (SRC), which assumes that noise also has a sparse representation, our sparse algorithm is developed based on the maximum correntropy criterion, which is much more insensitive to outliers. In order to develop a more tractable and practical approach, we in particular impose nonnegativity constraint on the variables in the maximum correntropy criterion and develop a half-quadratic optimization technique to approximately maximize the objective function in an alternating way so that the complex optimization problem is reduced to learning a sparse representation through a weighted linear least squares problem with nonnegativity constraint at each iteration. Our extensive experiments demonstrate that the proposed method is more robust and efficient in dealing with the occlusion and corruption problems in face recognition as compared to the related state-of-the-art methods. In particular, it shows that the proposed method can improve both recognition accuracy and receiver operator characteristic (ROC) curves, while the computational cost is much lower than the SRC algorithms.

Index Terms—Information theoretical learning, correntropy, linear least squares, half-quadratic optimization, sparse representation, M-estimator, face recognition, occlusion and corruption.

1 Introduction

Learning robust and discriminative face structure has been recognized as an important issue for real-world face recognition system. Well-known face recognition algorithms such as Eigenface [1], Fisherface [2], and Independent face [3] do not explicitly and effectively consider extracting robust facial features, although they are very useful for extracting descriptive or discriminative features.

To extract robust facial features, a number of algorithms, such as modular Eigenspaces [4], modular linear regression based classification (LRC) [5], eigenimages [6], [7], [8], minimax probability machine [9], reconstructive and discriminative subspace method [10], and associative memories [11], [12], were developed in order to achieve more robust performance of face recognition. To address the alignment problem of face images, De la Torre and Black developed the robust parameterized component analysis [13], which is also a modular Eigenspaces method, so that the performance such as face image reconstruction [13], Eigentracking [14], and active appearance models (AAM) [15] can be improved. Although notable improvement has been achieved by these methods, they can only deal with either the occlusion or corruption problem, or cannot deal with both of them very well. This is mostly because the effect of severe occlusion or corruption is not considered in these methods. In particular, some appearance models such as [14], [13] lack consideration of discriminant issues, and thus may be less discriminative for robust recognition under tough condition [10]. To eliminate the effect of occlusions, occlusion masks are incorporated to learn a robust classifier in [16], [17]. However, it needs to first properly determine the occlusion masks [16], [17], [10] and the occlusion masks may discard useful redundant information [18], [19] and might not be suitable for dealing with corruptions. Hence, learning a robust representation for face recognition is still challenging as any part of a face image could be corrupted in real-world scenarios and sometimes the magnitude of noise may be arbitrarily large.

Recently, sparse signal representation has shown significant potential in solving computer vision problems [20]. Typically, many sparse techniques are casted into an l^1 minimization problem, which is an approximately equal optimization problem to the l^0 minimization problem under certain conditions [21], [22]. Learning theory shows that it is enough to obtain good generalization if the number of nonzero weights of training samples that are used to encode a test sample is small as compared to the size of the training set [23]. Along this line, Wright et al. [24] recently proposed a sparse representation classifier (SRC) for robust face recognition against occlusions and corruptions, and impressive results were reported as compared to many well-known face recognition methods [1], [2], [25]. Although harnessing an "l^1norm" will lead to a well-structured

- *R. He is with the Institute of Automation, Chinese Academy of Sciences, 95 Zhongguancun East Road, Beijing 100190, China. E-mail: rhe@nlpr.ia.ac.cn.*
- *W.-S. Zheng is with the School of Information Science and Technology, Sun Yat-sen University, Guangzhou 510275, China. E-mail: wszheng@ieee.org.*
- *B.-G. Hu is with the Institute of Automation, Chinese Academy of Sciences, 95 Zhongguancun East Road, Beijing 100190, China. E-mail: hubg@nlpr.ia.ac.cn.*

Manuscript received 13 Nov. 2009; revised 3 May 2010; accepted 5 Oct. 2010; published online 30 Nov. 2010.
Recommended for acceptance by A. Martinez.
For information on obtaining reprints of this article, please send e-mail to: tpami@computer.org, and reference IEEECS Log Number TPAMI-2009-11-0760.
Digital Object Identifier no. 10.1109/TPAMI.2010.220.

algorithm and can theoretically guarantee its strong performance [26], the SRC algorithm is still not robust enough to contiguous occlusion for face recognition, as shown by Zhou et al. [18]. Furthermore, SRC would be hampered due to its expensive computational cost [24].

In this work, we propose to learn a robust sparse representation based on the correntropy [27] along with the use of an l^1 norm penalty. The correntropy has been shown to obtain robust analysis [19], [28] in information theoretic learning (ITL) [29], [30] and efficiently handle non-Gaussian noise and large outliers [27]. Those works show the connection between entropy and the Welsch M-estimator [31], [27], [28].

However, it is not easy to solve the optimization problem where the correntropy and l^1 norm penalty are co-operated. To address this computational problem, we propose a new algorithm by first imposing nonnegativity constraint on the variables in the correntropy. It not only greatly reduces the complexity of the model but also achieves significantly better performance as compared to the related state-of-the-art sparse algorithms for face recognition. Second, the half-quadratic (HQ) optimization technique is adopted to optimize the maximum correntropy criterion in an approximate way so that the optimization problem is further reduced to learning a sparse representation through a weighted linear least squares problem with nonnegativity constraint. A new active-set technique is also developed for fulfilling such an efficient method.

Our study of robustness and sparsity in the ITL framework for face recognition makes our work novel in the following aspects:

1. Robustness. Differently from SRC, which assumes that the noise term has a sparse representation, our correntropy-based sparse representation (CESR) is based on correntropy, which can efficiently cope with non-Gaussian noise and outliers [27]. To the best of our knowledge, it has achieved much better results than what has ever been reported for the challenging scarf occlusion problem in face recognition.
2. Sparsity. CESR is a novel model to solve the problem of recovering a nonnegative sparse signal. By imposing the nonnegativity constraint in CESR, we further find that the solution of CESR is effective and sparse enough.
3. Efficiency. By developing a half-quadratic algorithm for optimization, CSER is presented to be a much more efficient algorithm for learning a sparse representation of a face image for recognition as compared to the SRC methods.

Fig. 1 presents an overview of the proposed robust algorithm for face recognition. Fig. 1b gives a good illustration of the robustness of the proposed method. If a face is partially occluded, the pixels of the occluded parts will be assigned small weights, and thus affect the maximum correntropy objective function less. The learned sparse representation in Fig. 1c is informative and the reconstructed image in Fig. 1d is clear without occlusion.

The rest of this paper is structured as follows: We first briefly review existing linear representation and sparse representation methods for face recognition and discuss their limitations. In Section 3, we propose the CESR model and develop a half-quadratic based active set algorithm for its optimization. In Section 4, we discuss the sparsity and robustness of the proposed approach. In Section 5, the proposed approach is validated by conducting extensive experiments on the well-known and challenging face data sets along with the comparison with other related state-of-the-art techniques. Finally, we give the conclusion and discuss some future work in Section 6.

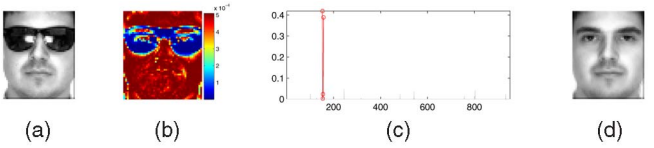

Fig. 1. Overview of our approach for robust face recognition. (a) A test face image with sunglasses occlusion. (b) The weight image learned by our approach. The entry with blue color has a small value, while the entry with red color has a large value. The larger the value of the entry, the more it contributes to the correntropy-based objective function. Due to the occlusion caused by the sunglasses, the pixels around the two eyes are assigned small weights, which means that they are estimated as noise. (c) The sparse coefficients computed by our approach. The red coefficients correspond to the training images with the same class label as the test image. Our algorithm finds the true identity from 952 training images of 119 individuals in the standard AR face database. (d) The reconstructed image by a learned sparse linear combination of all of the training images.

2 Related Works

A fundamental task in pattern recognition is to correctly classify a new test sample $y \in \mathbb{R}^{m\times 1}$ by using labeled training samples from k distinct classes. Let $X_c \doteq [x_1^c, x_2^c, \ldots, x_{n_c}^c] \in \mathbb{R}^{m\times n_c}$ be a data matrix which consists of n_c training samples (columns of X_c) from the cth class. Let x_{ij}^c and y_j be the jth entry of x_i^c and y, respectively. Given a sufficiently expressive training set X_c, a test image y of subject c can be approximated by a linear combination of given training samples, i.e., $y \approx X_c\beta^c$ for some coefficient vector $\beta^c \in \mathbb{R}^{n_c}$. By concatenating the training samples of all k classes, we get a new matrix X for the entire training set as: $X \doteq [X_1, X_2, \ldots, X_k] = [x_1^1, x_2^1, \ldots, x_{n_k}^k] \in \mathbb{R}^{m\times n}$, where $n = \sum_{c=1}^{k} n_c$. Alternatively, a test sample y can also be expressed as a linear combination of all training samples:

$$y \approx X\beta, \tag{1}$$

where the coefficient vector $\beta \in \mathbb{R}^n$. There are lots of works on learning this coefficient vector for face recognition. In the following we briefly review the major works.

2.1 Nonsparse Linear Classifier

To seek the best representation for the test sample y in class c, the nearest neighbor (NN) classifier finds the nearest training sample in that class. That is, it computes the minimal distance between y and all training samples of class c

$$r_c^{NN}(y) = \min_{x_i^c} \|y - x_i^c\|_2, \tag{2}$$

where $\|.\|_2$ denotes the l^2 norm.

Compared with the NN algorithm, linear representation methods seek the best representation by samples in each class. Among them, the simplest one is the nearest feature line (NFL) [32], which aims to extend the capacity of prototype features by computing a linear function to interpolate and extrapolating each sample pair belonging to the same class. In NFL, the distance is defined as follows:

$$r_c^{NFL}(y) = \min_{x_1^c, x_2^c, \beta_1} \left\| y - \beta_1 x_1^c + (1-\beta_1) x_2^c \right\|_2, \tag{3}$$

where $\beta_1 \in \mathbb{R}$. We can also rewrite (3) as follows:

$$r_c^{NFL}(y) = \min_{x_1^c, x_2^c, \beta_1, \beta_2} \left\| y - \left(\beta_1 x_1^c + \beta_2 x_2^c\right) \right\|_2 \quad s.t.\ \beta_1 + \beta_2 = 1. \tag{4}$$

If we extend (4) to a higher dimensional space, we get the following optimization problem:

$$r_c^{NCLC}(y) = \min_{\beta^c} \|y - X_c \beta^c\|_2 \quad s.t.\ \sum_{i=1}^{n_c} \beta_i^c = 1, \tag{5}$$

A local subspace classifier [33] solves (5) by assuming X_c is orthonormal. The nearest constrained linear combination (NCLC) algorithm [34] and K-Local hyperplane (HKNN) algorithm [35] solve (5) from a different geometric point of view. Note that by removing the equality constraint, we get

$$r_c^{NLC}(y) = \min_{\beta^c} \|y - X_c \beta^c\|_2. \tag{6}$$

The analytical solution of (6) can be directly computed by

$$\beta^c = (X_c^T X_c)^{-1} X_c^T y. \tag{7}$$

The nearest linear combination (NLC) [34] solves (6) by a pseudo-inverse matrix and LRC [5] solves (6) by (7). LRC simply makes use of the downsampled images for the LRC to achieve the state-of-the-art results as compared to the benchmark techniques [5]. The partial within-class match (PWCM) method [16], [17] solves (6) based on partial unterminated pixels. The PWCM further utilizes a robust classification metric based on a M-estimator when all β^c have been computed, i.e.,

$$\arg\min_c \|y - X_c \beta^c\|_r, \tag{8}$$

where $\|.\|_r$ is a robust norm based on M-estimators.

The minimal residual of (6) can also be taken as the distance from a query point to the space spanned by X_c. Then, we get the nearest feature space (NFS) algorithm [36] that computes the distance between a query point and its projected point onto the feature space

$$r_c^{NFS}(y) = \|y_p - y\|_2, \tag{9}$$

where y_p is the projection point of y onto the feature space spanned by X_c. According to (7), (6) can also be rewritten as

$$r_c^{NFS}(y) = \left\| y - X_c (X_c^T X_c)^{-1} X_c^T y \right\|_2. \tag{10}$$

If the columns of X_c are orthonormal, we have the nearest subspace algorithm [37] that solves the following optimization problem:

$$r_c^{NS}(y) = \left\| \left(I - X_c X_c^T\right) y \right\|_2. \tag{11}$$

After the residual or distance has been calculated, the label of the test sample y will be assigned $\arg\min_c r_c(y)$. Although those linear representation methods have indeed obtained promising improvement on performance, they still suffer two problems [24]:

1. The improvement of receiver operator characteristic (ROC) curve is quite limited.
2. They could not efficiently deal with the error incurred by severe occlusion and corruption.

2.2 Sparse Linear Classifier

Differently from traditional linear representation methods, the sparse representation-based classifier (SRC) [24] makes use of the discriminative nature of sparse representation to perform classification. Also, all samples in the training set are used in SRC to represent the test sample, which is different from the other well-known face recognition methods in the literatures. It aims to seek a sparse solution to (1) as follows:

$$\min \|\beta\|_0 \quad s.t. \quad y = X\beta, \tag{12}$$

where the l^0 norm $\|.\|_0$ counts the number of nonzero entries in a vector. Originally inspired by the theoretical analysis [21], [22] that the solution of the l^0 minimization problem is equal to the solution of the l^1 minimization problem under some conditions, SRC relaxes the above problem and seeks the sparse and informative vector β by solving the problem below

$$\min \|\beta\|_1 \quad s.t. \quad y = X\beta, \tag{13}$$

where $\|\beta\|_1 = \sum_{i=}^{n} |\beta_i|$. Here, we denote the model (13) by SRC0. In real-world face recognition applications, occlusions and corruptions are always incurred. Hence, the above linear model in (1) is modified as:

$$y = X\beta + e, \tag{14}$$

where $e \in \mathbb{R}^m$ is the error (noise) vector. By assuming that noise vector e also has a sparse representation, SRC seeks an approximation of the sparsest solution to (14):

$$\min \|\beta\|_1 + \|e\|_1 \quad s.t. \quad y = X\beta + e. \tag{15}$$

We denote the model (15) by SRC1.

Although SRC1 can effectively deal with the occlusion and corruption problems sometimes, it is still not robust enough to contiguous occlusion on facial images, as shown in [18]. In addition, SRC1 would be hampered due to its expensive computational cost [24]. For example, it will take nearly hundreds of seconds for SRC1 to process a test image represented by a 700D vector.

3 Correntropy-Based Sparse Representation

In this section, we first introduce correntropy, and then we propose a robust CESR for face recognition. A half-quadratic-based active set algorithm is also developed for optimization.

TABLE 1
Commonly Used M-Estimators and Their Corresponding Weight Functions

name	l^1	$l^1 - l^2$	Fair	Cauchy	German-McClure	Welsch
$\rho(x)$	$\lvert x\rvert$	$2(\sqrt{1+x^2/2}-1)$	$c^2\left[\frac{\lvert x\rvert}{c} - \log(1+\frac{\lvert x\rvert}{c})\right]$	$\frac{c^2}{2}\log(1+(x/c)^2)$	$\frac{x^2/2}{1+x^2}$	$\frac{c^2}{2}\left[1-\exp(-(x/c)^2)\right]$
$w(x)$	$\frac{1}{\lvert x\rvert}$	$\frac{1}{\sqrt{1+x^2/2}}$	$\frac{1}{1+\lvert x\rvert/c}$	$\frac{1}{1+(x/c)^2}$	$\frac{1}{(1+x^2)^2}$	$\exp(-(x/c)^2)$
$\hat{w}(x)$	$\frac{1}{\lvert x\rvert}$	$\frac{1}{\sqrt{1+x^2/2\sigma^2}}$	$\frac{1}{1+\lvert x\rvert/\sigma}$	$\frac{1}{1+(x/\sigma)^2}$	$\frac{1}{(1+x^2/\sigma^2)^2}$	$\exp(-(x/\sigma)^2)$

3.1 Correntropy

In real-world computer vision scenarios [7], [10], [24], face recognition against noise and outliers is critically challenging, mainly due to the unpredictable nature of the errors (bias) caused by those noise and outliers. That means where these errors exist in an image can differ for different test samples and is hard for computer to predict in advance. The errors may be arbitrarily large in magnitude, and therefore cannot be ignored or treated as small noise.

Recently, the concept of correntropy was proposed in ITL [27] to process non-Gaussian noise [27] and impulsive noise [38]. The correntropy is directly related to the Renyi's quadratic entropy [29] in which the Parzen windowing method is used to estimate the data distribution [39]. It is a local similarity measure between two arbitrary random variables A and B, defined by

$$V_\sigma(A,B) = E[k_\sigma(A-B)], \tag{16}$$

where $k_\sigma(.)$ is a kernel function that satisfies Mercer theory [40] and $E[.]$ is the expectation operator. It takes advantage of a kernel trick that nonlinearly maps the input space to a higher dimensional feature space. Differently from conventional kernel methods, it works independently with pairwise samples. With a clear theoretic foundation, the correntropy is symmetric, positive, and bounded.

In practice, the joint probability density function of A and B is often unknown and only a finite number of data $\{(A_j,B_j)\}_{j=1}^m$ are available. Hence, the sample estimator of correntropy is estimated by

$$\hat{V}_{m,\sigma}(A,B) = \frac{1}{m}\sum_{j=1}^{m} k_\sigma(A_j - B_j), \tag{17}$$

where k_σ is Gaussian kernel $g(x) \triangleq \exp(-\frac{x^2}{2\sigma^2})$.

Based on (17), Liu et al. [27], [41] further extended the sample-based correntropy criterion for a general similarity measurement between any two discrete vectors. That is, they introduced the correntropy induced metric (CIM) [27], [41] for any two vectors $A=(a_1,\ldots,a_m)^T$ and $B=(b_1,\ldots,b_m)^T$ as follows:

$$\begin{aligned} CIM(A,B) &= \left(g(0) - \frac{1}{m}\sum_{j=1}^{m} g(e_j)\right)^{\frac{1}{2}} \\ &= (g(0) - \frac{1}{m}\sum_{j=1}^{m} g(a_j-b_j))^{\frac{1}{2}}, \end{aligned} \tag{18}$$

where the error e_j is defined as $e_j = a_j - b_j$. For adaptive systems, the below correntropy of error e_j,

$$\max_\theta \frac{1}{m}\sum_{j=1}^{m} g(e_j), \tag{19}$$

is called the maximum correntropy criterion (MCC) [27], where θ is the parameter in the criterion to be specified later. MCC has a probabilistic meaning of maximizing the error probability density at the origin [41], and MCC adaptation is applicable in any noise environment when its distribution has the maximum at the origin [27]. Compared with the mean square error (MSE), a global metric, the correntropy is local. That means the correntropy value is mainly decided by the kernel function along the line $A=B$ [27].

Correntropy has a close relationship with M-estimators [42]. If we define $\rho(x) \triangleq 1-\exp(-x)$, (18) is a robust formulation of Welsch M-estimator [27]. Furthermore, $\rho(x)$ satisfies $\lim_{|x|\to\infty}\rho'(x)=0$, and thus it also belongs to the so-called redescending M-estimators [42], which have some special robustness properties [43]. A main merit of correntropy is that the kernel size controls all its properties. Due to the close relationship between m-estimation and methods of ITL, choosing an appropriate kernel size [27] in the correntropy criterion becomes practical.

Considering the relationship between correntropy and M-estimators, we further list several commonly used M-estimators ($\rho(x)$) and their corresponding weight functions $w(x)$ in Table 1 for further analysis.[1] We also introduce the kernel size into other M-estimators by substituting the x with x/σ and setting $c=1$. We denote the modified weight function by $\hat{w}(x)$. Our experimental results show that the kernel size for $\hat{w}(x)$ is also as effective as for correntropy.

3.2 The Proposed Model

For face recognition, let vector $A=(y_1,\ldots,y_m)^T$ be a facial image vector, and vector $B=(\sum_i x_{i1}\beta_i,\ldots,\sum_i x_{im}\beta_i)^T$ be a linear representation of data set X. We wish to find a sparse coding vector $\beta=(\beta_1,\ldots,\beta_n)^T$ such that B becomes as correlated to A as possible under the maximum correntropy criterion (19). Then, we have the following correntropy-based sparse model:

$$J_{CESR} = \max_\beta \sum_{j=1}^{m} g\left(y_j - \sum_{i=1}^{n} x_{ij}\beta_i\right) - \lambda\|\beta\|_1, \tag{20}$$

where $g(x)=\exp(-\frac{x^2}{2\sigma^2})$ is a Gaussian kernel function. Methods based on correntropy treat individual pixels of the representation differently and give more emphasis on those pixels corresponding to pixels of the same class as test

1. Although Huber's estimator can also be optimized by using the half-quadratic optimization, we do not discuss this estimator due to its threshold parameter. When there are noise and outliers, it is difficult to determine an appropriate value of the threshold.

sample y. This means if there are occlusions and corruptions in a test sample y, those pixels corresponding to outliers will have small contributions to the correntropy. Hence, the noise can be handled uniformly within the correntropy framework.

Efficient minimization of the l^1-norm based and related convex functions is an active area of research [44].[2] Generally, it is possible to optimize the correntropy criterion using the gradient descend technique if the l^1 penalty is not involved, albeit its usefulness is significant for pursuing sparsity. In view of this difficulty, we relax the above l^1 correntropy model by imposing a nonnegativity constraint on the coding vector β. We then get the following maximum correntropy problem:

$$J_{CESR} = \max_{\beta} \sum_{j=1}^{m} g\left(y_j - \sum_{i=1}^{n} x_{ij}\beta_i\right) - \lambda \sum_{i=1}^{n} \beta_i \quad s.t.\ \beta_i \geq 0. \tag{21}$$

We note the optimization problem in (21) as CESR.

Note that in SRC1, both two l^1-norm terms are approximations of l^0norm. The $\|e\|_1 = \|y - X\beta\|_1$ is an approximation of $\|y - X\beta\|_0$. Hence, the SRC1 assumes that the noise also has a sparse representation and tries to estimate and correct the error incurred by noise [24], [26]. However, the first part in (21) of CESR is actually a robust M-estimator. As analyzed later and illustrated in Fig. 1, CESR aims to detect the noise and utilize the unterminated data to yield a robust sparse representation.

In particular, we consider a special case when λ is set zero. The rationale of this special model is that the positive vector β is actually playing as a clustering indicator because each entry β_i reflects the importance of sample x_i in reconstructing pattern y. Hence, it should be expected that more weights would be assigned to the samples of the same class label of y, while weights of the others should be small and zero in the optimal case. Therefore, β can also be sparse in this case. When $\lambda > 0$, CESR can yield a sparser solution and further improve the recognition accuracy. We will further verify this scenario in experiment 5.7.

3.3 Algorithm of CESR

Since the objective function of CESR in (21) is nonlinear, CESR is difficult to directly optimize. Fortunately, we recognize that the half-quadratic technique [28] and expectation maximization (EM) method [45] can be utilized to solve this ITL based optimization problem. According to the property of convex conjugate function [46], we have:

Proposition 1. *There exists a convex conjugate function φ of $g(x)$[3] such that*

$$g(x) = \max_{p'} \left(p' \frac{\|x\|^2}{\sigma^2} - \varphi(p')\right), \tag{22}$$

and for a fixed x, the maximum is reached at $p' = -g(x)$ [28].

Substituting (22) into (21), we have the augmented objective function in an enlarged parameter space

$$\hat{J}_{CESR} = \max_{\beta,p} \sum_{j=1}^{m} \left(p_j \left(y_j - \sum_{i=1}^{n} x_{ij}\beta_i\right)^2 - \varphi(p_j)\right) - \lambda \sum_{i=1}^{n} \beta_i \quad s.t.\ \beta_i \geq 0, \tag{23}$$

where $p = [p_1, \ldots, p_m]^T$ are the auxiliary variables introduced by half-quadratic optimization. According to Proposition 1, for a fixed β, the following equation holds

$$J_{CESR}(\beta) = \max_{p} \hat{J}_{CESR}(\beta, p). \tag{24}$$

It follows that

$$\max_{\beta} J_{CESR}(\beta) = \max_{\beta,p} \hat{J}_{CESR}(\beta, p). \tag{25}$$

Then, we can conclude that maximizing $J_{CESR}(\beta)$ is identical to maximizing the augmented function $\hat{J}_{CESR}(\beta, p)$. Obviously, a local maximizer (β, p) can be calculated in an alternating maximization way

$$p_j^{t+1} = -g\left(y_j - \sum_{i=1}^{n} x_{ij}\beta_i^t\right), \tag{26}$$

$$\beta^{t+1} = \arg\max_{\beta} (y - X\beta)^T diag(p)(y - X\beta) - \lambda \sum_i \beta_i, \quad s.t.\ \beta_i \geq 0, \tag{27}$$

where t means the tth iteration and $diag(.)$ is an operator to convert the vector p to a diagonal matrix. It is clear that the optimization problem in (27) is a weighted linear least squares problem with nonnegativity constraint.[4] The auxiliary variables $-p$ can be viewed as weights in (27).

The optimal problem in (27) can be reformulated as the following quadratic program:

$$\min_{\beta} \left(\frac{\lambda}{2} - \hat{X}^T \hat{y}\right)^T \beta + \frac{1}{2}\beta^T \hat{X}^T \hat{X}\beta \qquad s.t.\ \beta_i \geq 0, \tag{28}$$

where $\hat{X} = diag(\sqrt{-p^{t+1}})X$ and $\hat{y} = diag(\sqrt{-p^{t+1}})y$. Since $\hat{X}^T\hat{X}$ is a positive semidefinite matrix, this quadratic program in (28) is convex. Based on the Karush-Kuhn-Tucker optimal conditions, the following monotone linear complementary problem (LCP) is derived [47]:

$$\alpha = \hat{X}^T\hat{X}\beta - \hat{X}^T\hat{y} + \frac{\lambda}{2}, \quad \alpha \geq 0,\ \beta \geq 0,\ \beta^T\alpha = 0, \tag{29}$$

If the matrix $\hat{X}$ has full column rank ($rank(\hat{X}) = n$), the convex program in (28) and the LCP in (29) have unique solutions for each vector $\hat{y}$ [47].

Let F and G be two subsets of $\{1, \ldots, n\}$ such that $F \cup G = \{1, \ldots, n\}$ and $F \cap G = \phi$. And let F and G be the working set and inactive set in the active set algorithm, respectively. Consider the following column partition of the matrix $\hat{X}$:

$$\hat{X} = [\hat{X}_F, \hat{X}_G], \tag{30}$$

2. In [44], the sparse solution of (13) is computed via solving the unconstrained optimization problem $J(\beta) + h(X\beta - y)$, where $J(.)$ is convex and $h(.)$ has to be convex and differentiable.

3. Strictly speaking, φ is the conjugate function of $exp(-x)$. Here, we harness the variable substitution method (substitute x with x^2/σ^2), which is commonly used in HQ.

4. According to Proposition 1, we can learn that $p \leq 0$. By replacing the p with $-p$, we can get the equivalent minimal problem.

where $\hat{X}_F \in \mathbb{R}^{m\times|F|}$, $\hat{X}_G \in \mathbb{R}^{m\times|G|}$, and $|F|$, $|G|$ are the number of F and G, respectively. We then can rewrite (29) as:

$$\begin{bmatrix}\alpha_F\\ \alpha_G\end{bmatrix} = \begin{bmatrix}\hat{X}_F^T\hat{X}_F & \hat{X}_F^T\hat{X}_G\\ \hat{X}_G^T\hat{X}_F & \hat{X}_G^T\hat{X}_G\end{bmatrix}\begin{bmatrix}\beta_F\\ \beta_G\end{bmatrix} - \begin{bmatrix}\hat{X}_F^T\hat{y}\\ \hat{X}_G^T\hat{y}\end{bmatrix} + \frac{\lambda}{2},$$

where $\beta_F,\ \alpha_F \in \mathbb{R}^{|F|}$, $\beta_G,\ \alpha_G \in \mathbb{R}^{|G|}$, $\beta = (\beta_F, \beta_G)$, and $\alpha = (\alpha_F, \alpha_G)$. Then, we can compute the values of variables β_F and α_G by the following iterative procedure [47]:

$$\min_{\beta_F\in R^{|F|}} \|\hat{X}_F\beta_F - \hat{y}\|_2^2 + \lambda\sum_{i\in F}\beta_i, \tag{31}$$

$$\alpha_G = \hat{X}_G^T(\hat{X}_F\beta_F - \hat{y}) + \frac{\lambda}{2}. \tag{32}$$

And the optimal solution is given by $\beta = (\beta_F, 0)$ and $\alpha = (0, \alpha_G)$. At each alternating maximum step in (27), instead of finding the optimal solution of the optimization problem, we simply learn a β in the feasible region to increase the objective. Combining (26), (31), and (32), we have the Half-Quadratic-based active-set algorithm for the proposed CESR model.

Algorithm 1 summarizes the optimization procedure. From Step 1 to Step 4, Algorithm 1 finds a feasible β to maximize the objective function for current p^t. In Step 5, Algorithm 1 computes the auxiliary variables of the Half-Quadratic optimization. It alternately maximizes the augmented objective function in (23) until it converges (Proposition 2). Note that Algorithm 1 may not reach the maximum value of the correntropy objective in (21) because it will return to Step 2 when a feasible solution occurs. Experimental results illustrate that this solution is good enough to achieve significant improvements over the related state-of-the-art methods.

Algorithm 1. Algorithm of CESR

Input: data matrix X, test sample y, $p^1 = -\mathbf{1}$, $F = \phi$, $G = \{1,\ldots,n\}$, $\beta = \mathbf{0}$, and $\alpha = -X^T y$.
Output: β

1: Compute $\hat{X} = diag(\sqrt{-p^t})X$ and $\hat{y} = diag(\sqrt{-p^t})y$.
2: Compute $r = \arg\min\{\alpha_i : i \in G\}$. If $\alpha_r < 0$, set $F = F \cup r$, $G = G - r$.
Otherwise stop: $\beta^* = \beta$ is the optimal solution.
3: Compute $\bar{\beta}_F$ by solving (31). If $\bar{\beta}_F \geq 0$, set $\beta^t = (\bar{\beta}_F, 0)$ and go to step 4.
Otherwise let r be such that:

$$\theta = \frac{-\beta_r}{\bar{\beta}_r - \beta_r} = \min\{\frac{-\beta_i}{\bar{\beta}_i - \beta_i} : i \in F \text{ and } \bar{\beta}_i < 0\}$$

and set $\beta^t = ((1-\theta)\beta_F + \theta\bar{\beta}_F,\ 0)$, $F = F - r$, $G = G \cup r$. Return to step 3.
4: Compute α according to (32).
5: Update the auxiliary vector p^{t+1} and kernel size σ according to (26) and (33) respectively. Return to step 1.

Like any kernel method, the selection of kernel size will affect the performance of the proposed technique, and kernel size is often determined empirically. In this study, the kernel size (bandwidth) is computed by

$$\sigma^2 = \frac{\theta}{2m}(X_F\beta_F - y)^T(X_F\beta_F - y), \tag{33}$$

where θ is a constant to control the noise. We set θ to 1 throughout the paper.

Proposition 2. *The sequence $\{\hat{J}_{CESR}(\beta^t, p^t), t = 1, 2, \ldots\}$ generated by CESR converges.*

Proof. According to (27) and Proposition 1, we have

$$\hat{J}_{CESR}(\beta^t, p^t) \leq \hat{J}_{CESR}(\beta^t, p^{t+1}) \leq \hat{J}_{CESR}(\beta^{t+1}, p^{t+1}).$$

The cost function increases at each alternating maximization step. Therefore, the sequence $\{\hat{J}_{CESR}(\beta^t, p^t),\ t = 1, 2, \ldots\}$ is nondecreasing. We can verify that $J_{CESR}(\beta)$ is bounded (property of correntropy [27]) and, by (25), $\hat{J}_{CESR}(\beta^t, p^t)$ is also bounded. Consequently, CESR converges. □

3.4 Classifier of CESR

We aim to classify an unseen sample y which comes from existing classes. Note that our criterion in (21) aims to reconstruct a test sample y using existing training samples as well as possible. Ideally, training samples from the same class of y should give the best reconstruction performance. This gives us the motivation to design a class specific reconstruction classifier similar to the sparse classifier proposed by [24], but the major difference is that the classifier introduced here is based on the correntropy criterion.

Therefore, we classify y as follows: For each class c, let $\delta_c : \mathbb{R}^n \to \mathbb{R}^{n_c}$ be a function which selects the coefficients belonging to class c, i.e., $\delta_c(\beta) \in \mathbb{R}^{n_c}$ is a vector whose entries are the entries in β corresponding to class c. Utilizing only the coefficients associated with class c, the given sample y is reconstructed as $\hat{y}_c = X_c\delta_c(\beta)$. Then, y can be classified by assigning it to the class c corresponding to the maximal nonlinear difference between y and $\hat{y}_c$, i.e.,

$$\max_c r_c(y) \doteq g(y - X_c\delta_c(\beta)), \tag{34}$$

where the kernel size σ in $g(x)$ is calculated by

$$\sigma^2 = \frac{\theta_r}{2k}\sum_{c=1}^{k}\|y - X_c\delta_c(\beta)\|_2^2. \tag{35}$$

We set θ_r to 1 throughout the paper. Algorithm 2, summarizes the classification procedure.

Algorithm 2. Classifier of CESR

Input: data matrix $X = [X_1, X_2, ..., X_k] \in \mathbb{R}^{m\times n}$ for k classes, a test sample $y \in \mathbb{R}^{m\times 1}$
Output: $identity(y)$

1: Solve the maximum correntropy problem ($\lambda = 0$):

$$\beta^* = \arg\max_\beta \sum_{j=1}^{m} g(y_j - \sum_{i=1}^{n} x_{ij}\beta_i) \quad s.t.\ \beta_i \geq 0$$

2: Calculate the residuals $r_c(y) = g(y - X_c\delta_c(\beta^*))$, for $c = 1, \ldots, k$
3: $identity(y) = \arg\max_c r_c(y)$

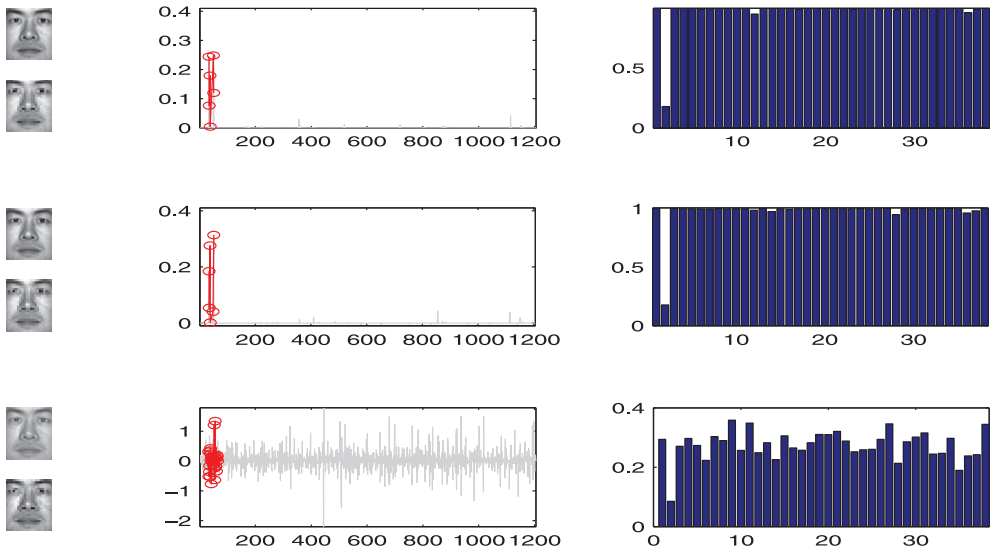

Fig. 2. Recognition using a 24×23 downsampled image as features. The image y belongs to subject 2 of Yale B. Left: The reconstructed images in original 192×168D feature space and downsampled 24×23D feature space, respectively. Middle: The coefficients computed by different algorithms. Nonzero coefficients associated with subject 2 are highlighted by deep color. Right: The residual ($r'_c(y) = \|y - X_c\delta_c(\beta)\|_2$) of the input image from subject 2. (a) The sparse representation of the CESR classifier. The ratio between the two smallest residuals in the right figure is about 1:5.4. (b) The sparse representation of SRC0. The ratio between the two smallest residuals in the right figure is about 1:5.3. (c) The linear representation of LRC. The ratio between the two smallest residuals in the right figure is about 1:2.2.

4 Sparsity and Robustness of CESR

In this section, we demonstrate the visual results of CESR for robust face recognition along with the comparison with SRC [24]. More results will be reported in the experiment section.

4.1 Sparsity of CESR

It has been shown that sparse representation is more efficient than the nonsparse one in many challenging cases for pattern analysis, as it is able to select the most representative training samples for representation of each test sample [23]. To show the strength of learning sparse features by CESR for face recognition, we compare it with SRC and show that the coefficients computed by CESR are more sparse and more effective. Results of LRC are also presented for reference.

We randomly selected half of the 2,414 images in the Extended Yale B database as the training set and the rest for testing, where the database will be introduced in the experiment section. The images are downsampled from the original size 192×168 to size 24×23.[5] As in [24], each image vector will have unit norm by normalization.[6]

The middle column in Fig. 2 shows the coefficients computed by different algorithms for a test image from the second subject in Yale database. The nonzero coefficients associated with subject 2 are highlighted by deep color. The numbers of nonzero coefficients (l^0 norm) computed by CESR, SRC0, and LRC are 28, 39, and 1,205, respectively. For CESR and LRC, we directly compute the number of nonzero coefficients. Since the coefficients of SRC0 solved by primal-dual algorithm have many small nonzero entries, we compute the number of nonzero coefficients of SRC0 by:

$$\|\beta\|_0^{SRC0} = \sum_{i=1}^{n} I(\beta_i), \tag{36}$$

where $I(x)$ is an indicator function:

$$I(x) = \begin{Bmatrix} 1 & |x| \geq \varepsilon \\ 0 & otherwise \end{Bmatrix}, \tag{37}$$

where $|.|$ is the absolute value operator. Here, we set $\varepsilon = 0.001$ to fairly compare different sparse methods. If we reduce the value of ε to a smaller value such as 0.0001, the number of nonzero entries computed by SRC0 will be larger than 100.

Fig. 5 further shows the average number of nonzero coefficients in the case of random corruption. (See experiment 5.32 for details of the setting.) We varied the percentage of corruption from 10 percent to 80 percent and computed the average numbers of nonzero coefficients. We find that CESR can also obtain sparse representations in this case and achieve much sparser representation than the one obtained by the l^1 norm based SRC1.

The right part of Fig. 2 shows the residuals $r'_c(y) = \|y - X_c\delta_c(\beta)\|_2$ with respect to the corresponding projected coefficients $\delta_c(\beta)$, $c = 1, \ldots, 38$. Like SRC0, CESR can correctly classify the test sample, where the dominant coefficients correspond to the second subject, which is of the same class as the test image. The ratios between the two smallest residuals of CESR, SRC0, and LRC are about 1:5.4, 1:5.3, and 1:2.2, respectively. The higher the ratio value, the more discriminative the algorithm can be. As we will show later in the experiment section, that higher ratio value also always implies a higher ROC curve.

The left part of Fig. 2 shows the reconstructed images in the original image space (top) and downsampled image space (bottom) using the coefficients learned by three different algorithms, respectively. For LRC, the coefficients associated with subject 2 are used to reconstruct the test

5. In [24], [5], face recognition methods make use of downsampled images as features to achieve impressive results.

6. In SRC [24], normalization is a necessary preprocessing step. Hence, we normalized the facial images to fairly compare different methods.

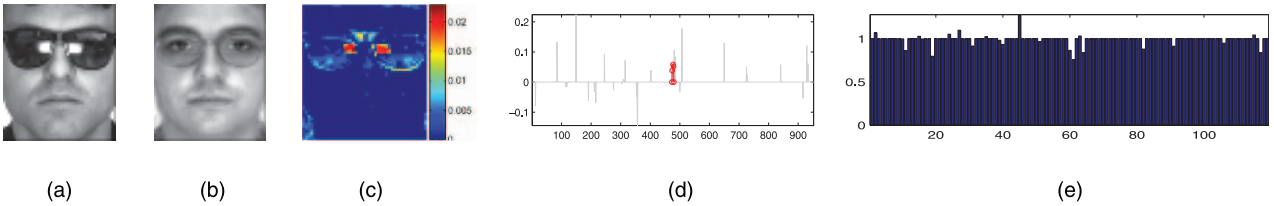

Fig. 3. Sparse representation computed by SRC1. (a) A test face image from the 60th subject in the AR database with sunglasses occlusion. (b) Reconstructed image as a sparse linear combination of all the training images. (c) The error image (by reshaping error vector e). The entry with red color has a large value, which means that this entry is estimated as noise by SRC1. (d) The sparse coefficients learned by SRC1. The red coefficients correspond to the training images with the same class label of the test image. (e) The residuals $r'_c(y)$ with respect to the coefficients for different classes. The minimal residual does not correspond to the same class of this test subject.

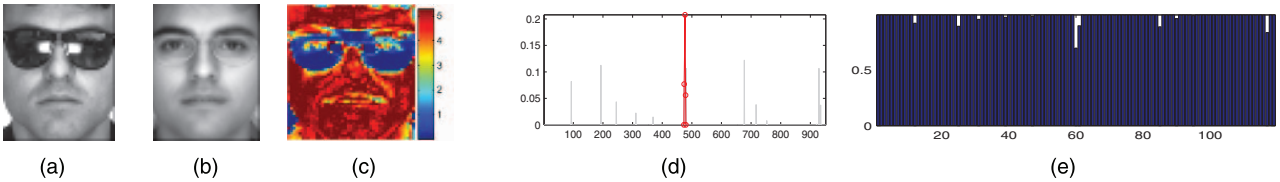

Fig. 4. Sparse representation computed by CESR. (a) The same occluded image as the one in Fig. 3. (b) The reconstructed image via a sparse linear combination of all of the training images. (c) The weight image (by reshaping auxiliary variable $-p$). The entry with blue color receives a small weight, which means that this entry is estimated as noise by CESR. (d) The sparse coefficients computed by CESR. The red coefficients correspond to the training images with the same class label of the test image and are the largest coefficients. (e) The residuals $r'_c(y)$ with respect to the coefficients for different classes.

image. Since the dominant coefficients of CESR and SRC0 are associated with subject 2, the reconstructed images are quite similar to the original images.

4.2 Robustness of CESR

In real-world applications, facial images always incur occlusions and corruptions. SRC1 presents a novel approach to deal with the errors caused by occlusions and corruptions by assuming that they also have sparse representations [24]. Although "sparse" may not mean "very few" [24], this assumption may make SRC1 fail when there are severe occlusions and corruptions. Fig. 3 shows such an example. As demonstrated in Fig. 3b, obvious shadows around the eyes can be found in the image reconstructed by SRC1. This is due to the inaccurate estimation of the noise. In Fig. 3a, the occlusion of sunglasses is roughly 20 percent. Fig. 3c further shows the noise item e in (15) when SRC1 converges (the e is reshaped to an image for visual illustration). Note that large entry value is marked in red color in the image. We can observe that only the two red regions in Fig. 3c corresponding to the two highlighted regions of sunglasses in Fig. 3a are estimated as noise. This inaccurate estimation makes the coefficients estimated by SRC1 less sparse and also less informative, so that the largest coefficients in Fig. 3d still contain much noisy information. This makes SRC1 fail to identify the correct subject in some cases.

However, CESR can correctly detect the occlusion in this scenario. As shown in Fig. 4b, the whole facial image is reconstructed much better by using CESR. The occluded regions around two eyes are also much clearer. Fig. 4c further shows the auxiliary variables $-p$ (we also reshape it to an image) in the Half-Quadratic optimization when CESR algorithm converges. We can find that the weights near two eyes have the lowest values, whereas others have large values, which makes CESR learn a robust sparse representation mainly from the nonoccluded region of facial images. Fig. 4d and 4e show the coefficients and residuals computed by CESR, respectively. Although the sunglasses occlude the area of two eyes, CESR classifier can still find the true identities (the 60th individual) from 952 training images of 119 individuals.

5 Experiment

To evaluate the proposed CESR algorithm, we compared it with two related state-of-the-art methods for robust face recognition: LRC and sparse representation-based classification (SRC). Experiments were performed on three public face recognition databases, namely, the AR [48], CMU [49], and FRGC [50] databases. The recognition rate, ROC curves, and computational cost of the compared methods will be reported. All algorithms were implemented in MATLAB on an AMD Quad-Core 1.80 GHz Windows XP machine with 2 GB memory.

5.1 Experimental Setting and Face Databases

Database. All gray-scale images of the three public face databases are aligned by the eyes' locations, which are manually located. Descriptions of the three databases are as follows:

1. *AR Database* [48]: The AR database consists of over 4,000 facial images from 126 subjects (70 men and 56 women). For each subject, 26 facial images are taken in two separate sessions. These images suffer different facial variations, including various facial expressions (neutral, smile, anger, and scream), illumination variations (left light on, right light on, and all side lights on), and occlusion by sunglasses or scarf. This database is always used for evaluating robust face recognition algorithm. In the experiment, we selected a subset of the data set that consists of 65 male subjects and 54 female subjects. The gray-scale images were resized to resolution 112×92.
2. *Extended Yale B Database* [49], [51]: The Extended Yale B database consists of 2,414 frontal face images from 38 subjects [49] under various lighting conditions. The cropped and normalized 192×168 face images were captured under various controlled

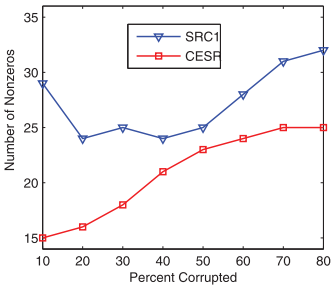

Fig. 5. Average numbers of nonzero coefficients with respect to different levels of random corruptions.

Fig. 6. **Cropped facial images of the first subject in AR database.** The images in the first row are from the first session and the images in the second row are from the second session.

lighting conditions [51], [24]. Fig. 7 shows some face images of the first subject in the Yale B database. For each subject, half of the images were randomly selected for training (i.e., about 32 images for each subject) and the rest were for testing.

3. *FRGC Database* [50]: The FRGC version two face database is a challenging benchmark face recognition database. There are 8,014 images from 466 subjects in the query set for FRGC experiment 4. These uncontrolled still images suffer variations of illumination, expression, time, and blurring. In our experiment, we only selected the objects which have over 10 facial images in the database, then got 3,160 facial images from 316 subjects. Each facial image was in gray scale and cropped into 32 pixel resolution by fixing the positions of two eyes. For each selected subject, eight images were randomly selected for training and the rest were for testing. Fig. 8 shows some images in the FRGC database.

Algorithm Setting. For SRC, we conducted its three models, which are different in the aspects of formulation and computational strategy. As suggested by [24], we implemented models of SRC by normalizing the facial image with unit norm. In our experiments, the details of these three models are:

1. *SRC0*: It minimizes the standard SRC in (12) via an active set algorithm based on [52].[7]
2. *SRC1*: It minimizes the l^1 norm in (38) via a primal-dual algorithm for linear programming based on [46], [53][8]

$$\min\|\beta\|_1 + \|e\|_1 \quad s.t. \quad \|y - X\beta + e\|_2 \leq \varepsilon, \qquad (38)$$

where ε is a given nonnegative error tolerance.

7. The MATLAB source code: http://redwood.berkeley.edu/bruno/sparsenet/.

8. The MATLAB source code: http://www.acm.caltech.edu/l1magic/.

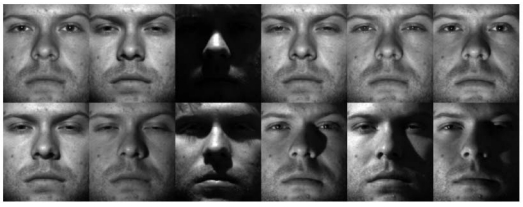

Fig. 7. Cropped facial images of one subject in the YALE B database.

Fig. 8. Cropped facial images of one subject in the FRGC database.

3. *SRC2*: In many cases, since the noise level ε in SRC1 is unknown beforehand [54], we can use the Lasso optimization algorithm to recover the sparse solution by[9]

$$\min\|y - X\beta + e\|_2^2 + \lambda(\|\beta\|_1 + \|e\|_1), \qquad (39)$$

where λ is a given regularization parameter which can be viewed as an inverse of the Lagrange multiplier associated with the constraint in (38). The ε can be interpreted as a pixel noise level, whereas λ cannot [24]. Since the noise level is also unknown in the testing set, the experimental results of SRC1 and SRC2 are not always the same due to different values of ε and λ.

In order to estimate the parameters ε and λ automatically, five-fold cross-validation on each dimension for each training set was used, where the candidate value set for both ε and λ is $\{1, 0.5, 0.25, 0.1, 0.075, 0.05, 0.025, 0.01, 0.005, 0.001, 0.0005, 0.0001\}$. Note that due to the large computational cost of SRC1 and SRC2, an exhaustive search of the parameter value is not feasible. Also, for the same reason, we can only report the experimental results of SRCs in the lower dimensional feature space.

For CESR, we mainly evaluated the proposed algorithm using the nonnegativity constraint with $\lambda = 0$. Discussion of λ will be given at the end of experiment section. More experimental results on parameter selection in CESR will be shown in Section 5.7 later.

5.2 Real-World Malicious Occlusion

We applied CESR to real face recognition scenarios against malicious occlusion.

5.2.1 Sunglasses Occlusion

For training, we used 952 nonoccluded frontal view images (about 8 for each subject) with varying facial expression. Fig. 6 shows an example of eight selected images of the first subject. For testing, we used images occluded by

9. The MATLAB source code: http://redwood.berkeley.edu/bruno/sparsenet/.

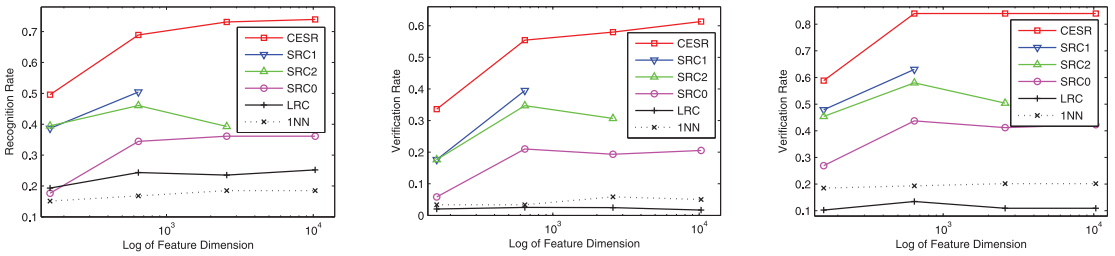

Fig. 9. Recognition rates and VR against sunglasses occlusion in the AR database. (a) Recognition rates. (b) $\mathrm{FAR} = 0.001$. (c) $\mathrm{FAR} = 0.01$.

sunglasses. Fig. 3a shows a facial image of the 60th individual from this testing set.

Fig. 9a shows the recognition performance of different methods using different downsampled images of dimensions 161, 644, 2,576, and 10,304. Those numbers correspond to downsampling ratios of 1/8, 1/4, 1/2, and 1, respectively. We see that if occlusions exist, it is unlikely that the test image will be very close to any single training image of the same class, so that the NN classifier performs poorly. Although SRC0 and LRC can improve the recognition rates compared to 1NN, their improvements are limited because they are based on the MSE criterion, which is sensitive to outliers. As illustrated in Fig. 4, CESR can model the noise more accurately, and therefore, perform significantly better.

The ROC curve is also illustrated in Fig. 9. ROC is important for evaluating different methods for face recognition in order to measure the accuracy of outlier rejection. A good algorithm should achieve a high-verification rate (VR) at a very low false acceptance rate (FAR). In a face recognition system, users often care about the VR when the FAR are 0.001 and 0.01 [55]. Fig. 9b and 9c show the VR when $\mathrm{FAR} = 0.001$ and $\mathrm{FAR} = 0.01$, respectively. The VR of 1NN and LRC are quite low. Although LRC has better recognition performance than 1NN, LRC cannot get better ROC curves and the VR of LRC is even lower than that of 1NN. Still the VR of CESR is the highest among the compared methods as shown.

5.2.2 Scarf Occlusion

For training, we used 952 nonoccluded frontal view images (about eight for each subject) with varying facial expression. Fig. 6 shows an example of eight selected images of the first subject. For testing, we used images with a scarf (one image for each person), which makes the facial image roughly 45 percent occluded. Fig. 10a shows a facial image of the first subject from this testing set.

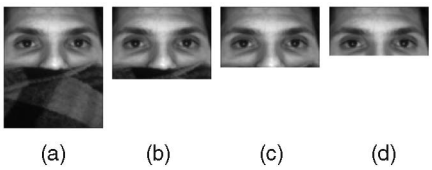

Fig. 10. Samples of cropped faces with scarf occlusion from the AR database. (a) Cropped images of the first subject. (b) 40 percent pixels (white region) are treated as missing pixels. (c) 50 percent pixels are treated as missing pixels. (d) 60 percent pixels are treated as missing pixels.

In the case of scarf occlusion, we can treat the region occluded by the scarf as missing pixels. Fig. 10b, 10c, and 10d show different levels of missing pixels. In real-world face recognition systems, we often need to manually crop the facial image when there is severe and continuous occlusion. For example, the mouth in a face image is occluded by a scarf [5]. It is convenient for users to simply locate the continuous occlusion as a rectangle region during manual alignment. In view of this, during the optimization of CESR, the entries of the auxiliary variable p corresponding to the missing pixels would be set zero.

Table 2 tabulates the recognition rates of our approach using various feature spaces (downsampled images) at different levels of missing values. To the best of our knowledge, the recognition accuracy 98.3 percent obtained by the proposed approach is probably the best result that has ever been reported against scarf occlusion. Note that for 100 subjects, the previous best results were 95.5 percent and 93.5 percent obtained by the SRC approach [24] and modular LRC approach in [5], respectively, and for 50 subjects, it was 93 percent reported in [10].

Fig. 11 further shows the recognition rates with respect to different levels of missing pixels when the size of image is 54×46. Our proposed maximum correntropy framework shows a quite stable performance against scarf occlusion and achieves the highest performance as well.

TABLE 2
Recognition Rates (Percent) for
Various Feature Spaces and Different Levels of Missing Values

Missing pixels	14×11	28×23	54 × 46
60%	85.71%	93.28%	93.28%
50%	90.76%	97.48%	**98.32%**
40%	91.60%	95.80%	95.80%

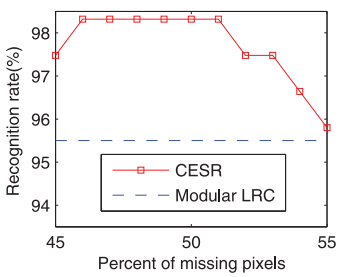

Fig. 11. Recognition rates against scarf occlusion under different levels of missing pixels. The size of the image is 54×46.

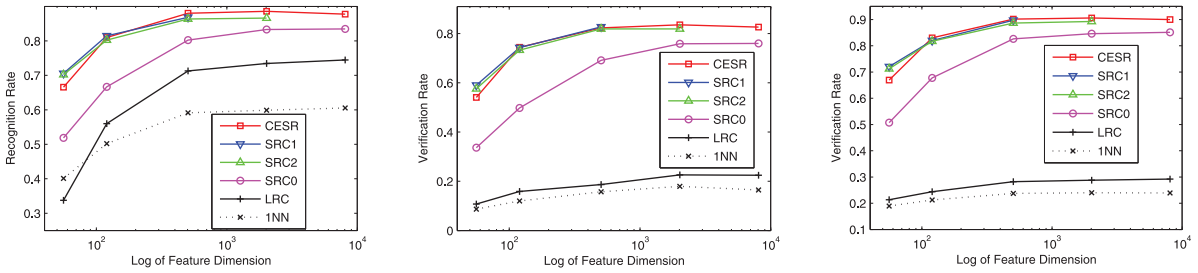

Fig. 12. Recognition rates and VR using various feature spaces and classifiers against 20 percent of contiguous occlusions. (a) Recognition rates. (b) $FAR = 0.001$. (c) $FAR = 0.01$.

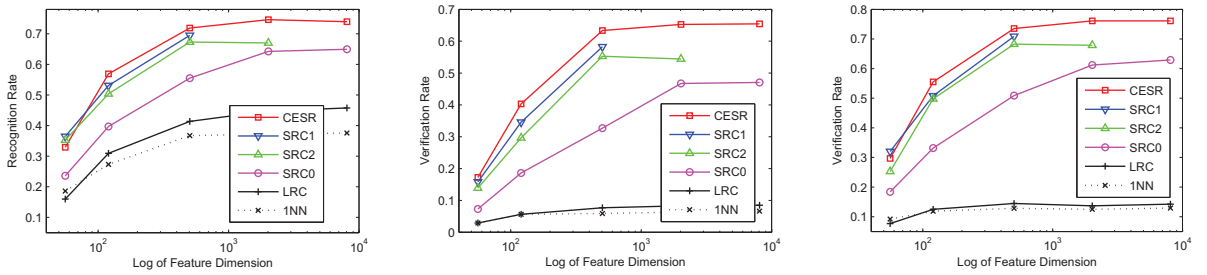

Fig. 13. Recognition rates and VR using various feature spaces and classifiers against 40 percent contiguous occlusions. (a) Recognition rates. (b) $FAR = 0.001$. (c) $FAR = 0.01$.

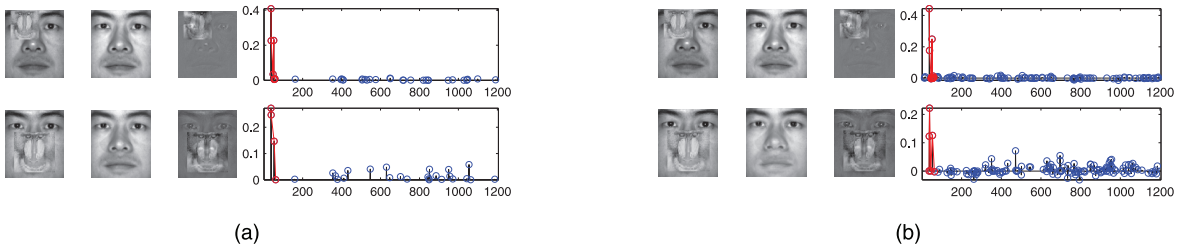

Fig. 14. Sparse representations by CESR and SRC against contiguous occlusion. The top row is with 20 percent occlusion and the bottom row is with 40 percent occlusion. The red entries of coefficients correspond to training images of the same person as the test image. (a) Sparse representation by CESR. Pictures from left to right are occluded images, the reconstructed images by using CESR, the difference image between original image and the reconstructed image, and the coefficients computed by CESR, respectively. (b) Sparse representation by SRC1. Pictures from left to right are occluded images, the reconstructed images by using SRC1, the difference image between original image and the reconstructed image, and the coefficients computed by SRC1, respectively.

5.3 Contiguous Occlusion and Corruption

5.3.1 Contiguous Occlusion of Random Block

In this section, we simulated various types of contiguous occlusion by replacing a randomly selected local region in each test image with an unrelated image [24]. Two images (top and bottom) in Fig. 14a show two occluded images with 20 percent and 40 percent occlusions by monkey images, respectively. Since the pixels of the unrelated monkey image are similar to the pixels of human face image, this contiguous occlusion is more challenging than the occlusion caused by random black or white dots.

We extensively evaluated different methods on the Extended Yale B Face Database against such a kind of contiguous occlusion. For each subject, half of the images were randomly selected for training (i.e., about 32 images for each subject), and the remaining half were for testing, and the training set and the testing set contained 1,205 and 1,209 images, respectively. We computed recognition rates with respect to five feature (downsampled image) spaces of dimensions 56, 120, 504, 2,016, and 8,064. Those numbers correspond to the downsampling rates of 1/24, 1/16, 1/8, 1/4, and 1/2, respectively.

Fig. 12a and Fig. 13a show the recognition accuracy with respect to different feature spaces. CESR achieves the highest recognition rates (88.6 percent and 74.6 percent) on the dimension of 8,064 where face images are with 20 percent and 40 percent occlusions. We note that SRC1 can slightly outperform CESR on the 56D space. This may be due to the nonoptimality of the kernel size in the correntropy. As will be demonstrated in Section 5.7, a well-tuned kernel size can further improve the recognition rate. Though SRC0 and LRC can also improve the recognition rates, their improvements are not good enough as compared with the other three robust methods. The verification results are also shown in Fig. 12 and Fig. 13. CESR is still overall better than the compared methods, especially when the occlusion is 40 percent.

Moreover, CESR can obtain much sparser coding. Fig. 14 shows two representative results of CESR and SRC1 against contiguous occlusions. In both examples (with 20 percent and

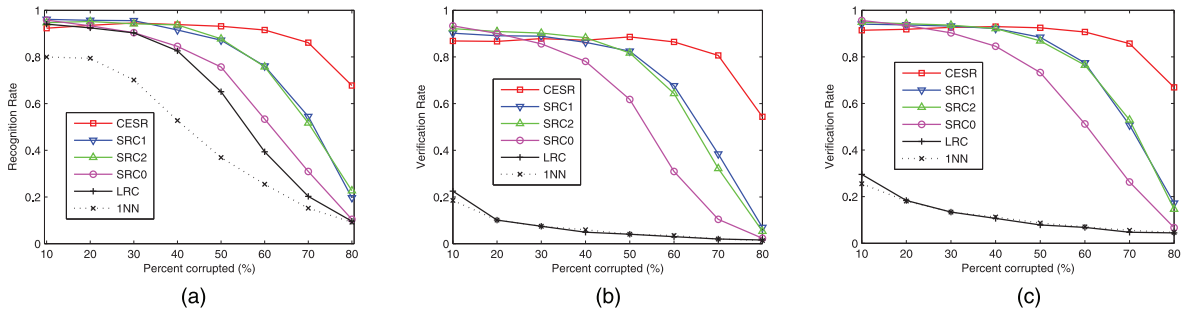

Fig. 15. Recognition rates and VR against random corruption using various classifiers. CESR significantly outperforms the others when there are severe corruptions. (a) Recognition rates. (b) VR when $\mathrm{FAR} = 0.001$. (c) VR when $\mathrm{FAR} = 0.01$.

40 percent occlusions, respectively), the estimated coefficients of CESR are sparser than the ones estimated by SRC1. Also, CESR is more efficient than SRC1. When the dimension is $2{,}016$-D (48×42), SRC1 takes nearly *800* seconds for computation of each test image on Matlab, while CESR only takes about 11 seconds.

5.3.2 Corruption

In practical face recognition scenarios, the test image y could be partially corrupted. We tested the robustness of CESR on the Extended Yale B Face Database. For each subject, half of the images were randomly selected for training and the remaining half were for testing. The training and testing set contained 1,205 and 1,209 images, respectively. Since the images in the testing set have large variations due to different lighting conditions or facial expressions, it is a difficult recognition task. For CESR, SRC2, SRC0, LRC, and 1NN, all of the images were resized to 48×42; for SRC1, we had to resize each image to 24×21 and stacked it into a 504D vector because running SRC1 on high-dimensional space is extremely expensive (if not impossible). Each test image was corrupted by replacing a set of randomly selected pixels with random pixel value, which follows a uniform distribution over $[0, 255]$. We varied the percentage of entire image pixels that will suffer corruption from 10 percent to 80 percent.

Fig. 15a shows the recognition accuracies of CESR and its five competitors with respect to different levels of corruption. CESR dramatically outperforms the others when the corruption is beyond 50 percent. With 80 percent corruption, the recognition rate of CESR is still 67.7 percent, whereas none of the other compared methods achieves higher than 25 percent recognition rate. If the parameter of CESR is well tuned, its recognition rate can reach 80.3 percent (see Fig. 19c) against 80 percent corruption. Note that compared with the two robust SRCs, the improvement in terms of recognition rate by CESR is nearly 45 percent.

Fig. 15b and 15c further show the VR with respect to various corruptions when $\mathrm{FAR} = 0.001$ and $\mathrm{FAR} = 0.01$. Although LRC can obtain 90 percent recognition rate when the corruption is smaller than 30 percent, its VR are extremely low (smaller than 30 percent). In contrast, CESR, SRC1, and SRC2 can significantly improve the ROC curves as they all seek sparse representation. When the corruption is larger than 50 percent, the VR of CESR are significantly higher than the others. Thus, CESR could be an effective method to deal with severe corruption for face recognition.

5.4 Results on the FRGC Database

In this section, we evaluated different methods on real facial images collected from uncontrolled conditions. We made use of a subset of the query set for FRGC experiment 4. The FRGC version 2 face database is a challenging benchmark face recognition database. Two scenarios have been considered: 1) In the first scenario, for each selected subject, eight images were randomly selected for training and the rest were for testing. 2) In the second scenario, we considered a real occlusion problem incurred in automatic face recognition system, especially in a surveillance or infrared face recognition system. Note that when a person's face is close to the border of the camera [56], a face alignment program may only crop part of the face, and therefore the missing part needs to be fixed. To simulate this kind of cropping error, we randomly blocked each testing image by a rectangle near the image border.

For the first scenario, the recognition rates of the five compared methods are shown in Fig. 16a as the functions of the number of feature dimensions. We see that the compared methods can be ranked in terms of ascending recognition rates by LRC, SRC1, SRC2, SRC0, and CESR. Although the improvement of CESR is limited, it can achieve a higher recognition rate with a small computation cost as compared to the SRC methods.

For the second scenario, we compared recognition rates against different levels of cropping error. Results are shown in Fig. 16b. We see that the recognition rates of both LRC and SRC0 drop fast as the level of cropping error increases. However, the three robust sparse methods can still obtain high-recognition rates. As expected, CESR can detect the cropping occlusion well so that it achieves the highest recognition rates.

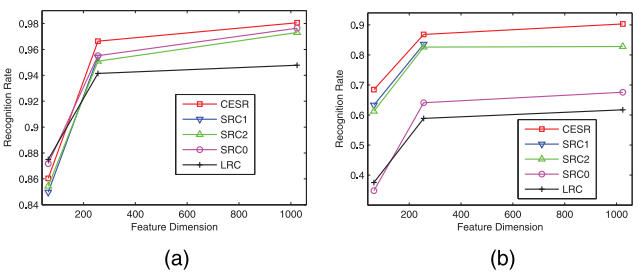

Fig. 16. Recognition rates of various classifiers on the FRGC database. (a) Original images. (b) Cropping occlusion.

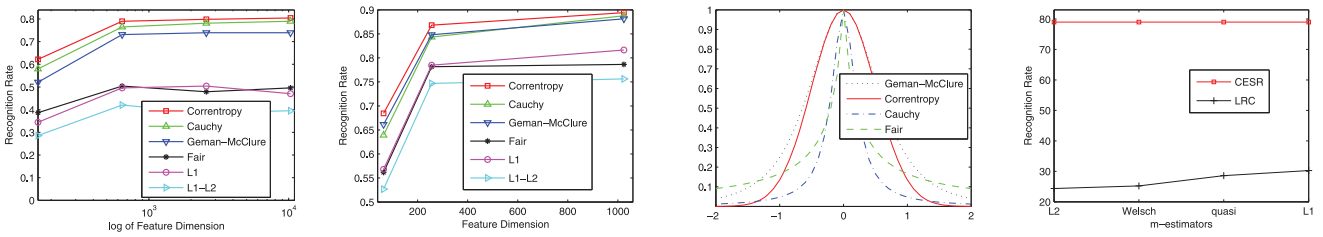

Fig. 17. Recognition rates of Algorithm 1 based on different M-estimators. (a) The recognition rates on the AR database. The experimental setting is the same as that in section 5.2.1. (b) The recognition rates on the FRGC database. The experimental setting is the same as that of the cropping occlusion in Section 5.4. (c) Weight functions of different M-estimators using the best-tuned parameter. (d) The recognition rates of CESR and LRC based on (8) on the AR database.

5.5 M-Estimators

Considering that the weight functions of "$l^1 - l^2$" and "Fair" in Table 1 are exactly the minimizer functions relevant to the multiplicative form of the HQ [57], we can directly substitute the objective in (21) with "$l^1 - l^2$" and "Fair" M-estimators. The simple modification of Algorithm 1 is to substitute the minimizer function in (26) with other minimizer functions. Note that not all M-estimators can be optimized by half-quadratic technique. An estimator should satisfy some conditions as detailed in [57], and then can be optimized by the multiplicative form of the HQ. In order to evaluate different M-estimators, we still substituted the minimizer function in (26) with other weight functions of the "l^1," "Cauchy," and "German-McClure" M-estimators. For each M-estimator, the results reported here are with the best tuned θ in set {2, 1.5, 1, 1/2, 1/5, 1/10, 1/20, 1/30, 1/40, 1/50}. The best values of θ for correntropy, "Cauchy," "German-McClure," "Fair," and "$l^1 - l^2$" are 0.5, 0.05, 1, 0.2, and 0.025, respectively.

Figs. 17a and 17b show the recognition rates on AR database and FRGC database, respectively. We see that the recognition rates of correntropy, "Cauchy," and "German-McClure" are higher than those of "Fair," "l^1," and "$l^1 - l^2$" on the two databases. Furthermore, the recognition rates of correntropy, "Cauchy," and "German-McClure" are very close. To further investigate the relationship among different M-estimators, we show the weight functions (or minimizer functions) of different M-estimators using the best tuned parameter in Fig. 17c. We see that the weight function of "German-McClure" is similar to that of correntropy. The reason that correntropy can outperform "German-McClure" may be because the weight function of "German-McClure" assigns outliers larger weights. By comparing with "Cauchy" and "Fair," we see that the weight function of "Fair" also gives outliers larger weights so that the algorithm based on "Fair" could not achieve a higher recognition rate. Therefore, according to the recognition rate and parameter selection, the correntropy is preferred, at least for our problem compared to other M-estimators.

In the partial within-class match (PWCM) method [16], [17], the l^1 norm and 0.5-quasi norm were used in (8) as robust estimator of classifier to further improve the classification performance after the coefficient has been computed. For further investigation, we implemented the classifiers of LRC and CESR by utilizing the "Welsch" M-estimator, l^1 norm, and 0.5-quasi norm as the robust norm in (8). Fig. 17d shows comparison results of the recognition rates between LRC and CESR. We see that the recognition rates of LRC increase when the robust estimators are used in the classifier. However, the recognition rates of CESR are nearly the same. This may be due to the fact that the robust estimator of classifiers do not change the sparse coefficients computed by CESR dramatically and also the nonnegative sparse representation is informative enough for classification.

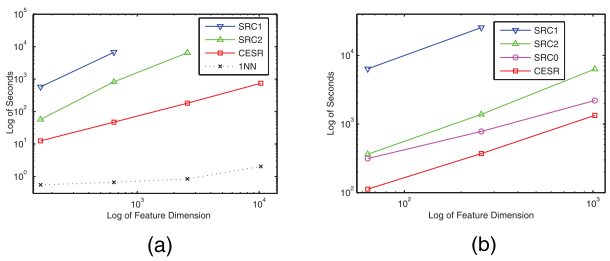

Fig. 18. Computational cost on various feature spaces and classifiers. (a) There are 952 images (eight images per subject) in the training set on AR database. (b) There are 2,528 images (eight images per subject) in the training set on FRGC database.

5.6 Comparison of the Computation Expense

The computational complexity of an algorithm is an important issue for face recognition. Fig. 18a shows the overall computation time using various features on the AR database with the same experiment setting as in Section 5.2.1. And Fig. 18b shows the overall computation time using various features on FRGC database, with the same experiment setting in Section 5.4. On the AR database, SRC1, SRC2, and CESR take 56, 6.9, and 0.40 seconds for each test image, respectively, when the feature dimension is 644D. (In [24], SRC1 requires about 75 seconds per test image on a PowerMac G5.) Hence, the computation time of two SRC methods is extremely large as compared to CESR. Although there are n linear variables and m auxiliary variables in CESR, CESR can efficiently estimate the m auxiliary variables in half-quadratic optimization. At each iteration, all of the m auxiliary variables are updated by (26) according to Proposition 1. However, the SRC models treat $m + n$ variables equally. When the dimension m is large, the computation cost of SRCs will increase rapidly and become extremely expensive.[10] Hence, CESR is more suitable for robust and real-time pattern recognition tasks.

10. Although, SRC methods may be used on down-sampled images to reduce its computation cost, both its recognition and verification performances will decrease significantly if the resolution of down-sampled images is too small.

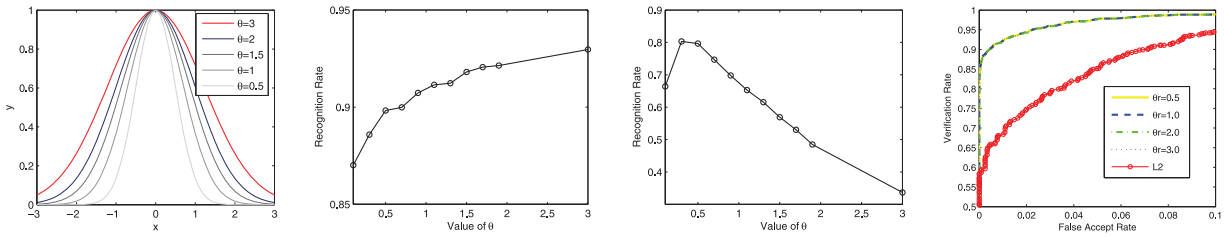

(a) (b) (c) (d)

Fig. 19. Recognition performance versus θ in Gaussian kernel size σ. (a) Gaussian function $y = exp(-x^2/\theta)$ as a function of θ. (b) On 10 percent corruption, the recognition rate under various values of θ. (c) On 80 percent corruption, the recognition rate under various values of θ. (d) On 10 percent corruption, the ROC curves under various values of θ_r. The L_2 represents that the scores are computed by L_2 distance.

5.7 Parameter Selection

5.7.1 Kernel Size σ

The kernel size σ is an important parameter, which controls all robust properties of correntropy [27]. A well-tuned kernel size value can eliminate the effect of outliers and noise much more effectively.

In this paper, we set the Gaussian kernel size as a single function of the average reconstruction error (defined in (33)). When the half-quadratic optimization is used to solve the correntropy, the correntropy will give outliers much smaller weights during iterations. The values of auxiliary variables (weights) are also computed by the Gaussian kernel function. A graphical description of this mechanism is given by plotting the Gaussian function as a function of the θ (see Fig. 19a). When the value of θ is small, such as 0.5, the outliers will receive much smaller weights. When the value of θ is large, such as 3, the outliers will receive relatively larger weights.

The simulations (see Fig. 19b and Fig. 19c) were run to show how the kernel size affects the performance of CESR under various corruptions. The experimental setting is the same as that in Section 5.3.2. On 10 percent corruption, the larger the θ, the higher the recognition rate that CESR obtains. The margin between the maximum recognition rate and the minimum is 6 percent. On 80 percent corruption, CESR achieves the highest recognition rate when $\theta = 0.5$. The margin between the maximum recognition rate and the minimum is 46 percent. When the percentage of corruption or occlusion is smaller than 50 percent, the average reconstruction error in (33) is mainly dominated by uncorrupted pixels, and therefore θ can be set to a larger value to give most of the uncorrupted pixels larger weights; when the corruption or occlusion is larger than 50 percent, the average reconstruction error is mainly dominated by corrupted pixels, and therefore θ can be set to a smaller value to punish outliers significantly.

Fig. 19d shows the ROC curves with different values of θ_r in (35). It seems that the verification performance of CESR is robust to different θ_r. Furthermore, the nonlinear scores learned by (34) can significantly improve the ROC curves compared with the scores (residuals) based on L_2 distance.

5.7.2 Regularization Parameter λ

The regularization parameter λ in (21) is an important parameter to control the sparseness of sparse representation. We study how the λ affects recognition rates in the case of sunglasses occlusion on the AR database and cropping occlusion on the FRGC database. We specially normalized the columns of X to have unit l^2 norm so that we can easily tune the regularization parameter λ of CESR.

Table 3 reports the recognition rates (percent) and average number of nonzero entries of the learned sparse representation (in terms of l^0 norm) when different values of λ are set. When we vary the value of λ from 0 to 0.05 on the AR database, the average number of nonzero entries decreases on both downsampling rates. This means that a larger value of λ will lead a more sparse solution. However, the sparsest solution may not yield the highest recognition rate. When λ is 0.05, the recognition rates under the two downsampling rates are only 26.05 percent and 25.21 percent on the AR database, respectively.

On the FRGC database, we also observe that recognition rates can be further improved if λ in CESR is well tuned. This is because λ controls the sparsity of coefficient β. When the data is redundant, an appropriate value of λ makes the sparse representation more informative.

6 Conclusion and Future Works

An effective sparse representation algorithm based on the maximum correntropy criterion is proposed for robust face recognition. The half-quadratic optimization technique is adopted to maximize the correntropy objective function, so that the difficult nonlinear optimization problem is reduced to learning a nonnegative representation through a weighted linear least squares problem with nonnegativity constraint at each iteration. Then a new active-set algorithm is developed to efficiently solve CESR. The sparse representation computed by CESR is robust to noise and can be computed more efficiently as compared to an l^1 norm-based sparse algorithm. A classifier based on the sparse representation is proposed for robust face recognition. Experimental results show that CESR is able to provide new

TABLE 3
Recognition Rates (Percent) and Average Number of Nonzeros (l^0 $norm$) under Different Values of λ

Value of λ	0	$1e^{-5}$	$1e^{-4}$	0.001	0.01	0.05
	Image size 28 × 23 (AR database)					
Recognition rates	68.91	**69.75**	**69.75**	**69.75**	68.07	26.05
l^0 $norm$	10.55	10.55	10.54	10.50	9.92	5.88
	Image size 56 × 46 (AR database)					
Recognition rates	**73.11**	**73.11**	**73.11**	72.27	68.07	25.21
l^0 $norm$	10.94	10.94	10.88	10.77	9.66	5.91
	Image size 16 × 16 (FRGC database)					
Recognition rates	86.81	86.81	**88.55**	47.15	0.3	0
l^0 $norm$	15.31	15.04	12.54	4.28	0	0

advanced ability to deal with errors caused by occlusions, corruptions and, etc., and can achieve striking recognition performance in tough conditions.

The correntropy-based sparse framework is presented to be a novel way to learn robust and informative presentations in this paper. This could suggest that improvement could be made if it is applied to learn an informative graph [28] for graph-based machine learning tasks such as data clustering, subspace learning, and semi-supervised learning, where the MSE criterion is still widely used in these algorithms. As robustness is an important issue for signal classification [58], image classification [59], and real-time object detection [24], we expect to investigate more use of the (maximum) correntropy criterion for these applications in future.

ACKNOWLEDGMENTS

The authors would like to greatly thank the associate editor and the reviewers for their valuable comments and advice. This work was supported in part by DUT R&D start-up costs, the Natural Science of Foundation of China (#61075051), and the NSFC-GuangDong (U0835005), and the 985 Project at Sun Yat-sen University under Grant no. 35000-3181305. Wei-Shi Zheng was with Department of Computer Science, Queen Mary University of London.

REFERENCES

[1] M. Turk and A. Pentland, "Eigenfaces for Recognition," *J. Cognitive Neurosicence,* vol. 3, no. 1, pp. 71-86, 1991.

[2] P.N. Belhumeur, J. Hespanha, and D.J. Kriegman, "Eigenfaces versus Fisherfaces: Recognition Using Class Specific Linear Projection," *IEEE Trans. Pattern Analysis and Machine Intelligence,* vol. 19, no. 7, pp. 711-720, July 1997.

[3] J. Kim, J. Choi, J. Yi, and M. Turk, "Effective Representation Using ICA for Face Recognition Robust to Local Distortion and Partial Occlusion," *IEEE Trans. Pattern Analysis and Machine Intelligence,* vol. 27, no. 12, pp. 1977-1981, Dec. 2005.

[4] A. Pentland, B. Moghaddam, and T. Starner, "View-Based and Modular Eigenspaces for Face Recognition," Technical Report 245, 1994.

[5] I. Naseem, R. Togneri, and M. Bennamoun, "Linear Regression for Face Recognition," *IEEE Trans. Pattern Analysis and Machine Intelligence,* vol. 32, no. 11, pp. 2106-2112, Nov. 2010.

[6] A. Leonardis and H. Bischof, "Robust Recognition Using Eigenimages," *Computer Vision and Image Understanding,* vol. 78, no. 1, pp. 99-118, 2000.

[7] A.M. Martinez, "Recognizing Imprecisely Localized, Partially Occluded, and Expression Variant Faces from a Single Sample Per Class," *IEEE Trans. Pattern Analysis and Machine Intelligence,* vol. 24, no. 6, pp. 748-763, June 2002.

[8] S. Chen, T. Shan, and B.C. Lovell, "Robust Face Recognition in Rotated Eigenspaces," *Proc. Int'l Image and Vision Computing New Zealand Conf.,* 2007.

[9] C.H. Hoi and M.R. Lyu, "Robust Face Recognition Using Minimax Probability Machine," *Proc. IEEE Int'l Conf. Multimedia and Expo,* pp. 1175-1178, 2004.

[10] S. Fidler, D. Skocaj, and A. Leonardis, "Combining Reconstructive and Discriminative Subspace Methods for Robust Classification and Regression by Subsampling," *IEEE Trans. Pattern Analysis and Machine Intelligence,* vol. 28, no. 3, pp. 337-350, Mar. 2006.

[11] R.A. Vazquez, H. Sossa, and B.A. Garro, "Low Frequency Response and Random Feature Selection Applied to Face Recognition," *Proc. Int'l Conf. Image Analysis and Recognition,* 2007.

[12] R.A. Vazquez and H. Sossa, "Associative Memories Applied to Pattern Recognition," *Proc. Int'l Conf. Artificial Neural Networks,* pp. 111-120, 2008.

[13] F. de la Torre and M.J. Black, "Robust Parameterized Component Analysis: Theory and Applications to 2D Facial Appearance Models," *Computer Vision and Image Understanding,* vol. 91, pp. 53-71, 2003.

[14] M. Black and A. Jepson, "Eigentracking: Robust Matching and Tracking of Articulated Objects Using a View-Based Representation," *Int'l J. Computer Vision,* vol. 26, no. 1, pp. 63-84, 1998.

[15] T. Cootes, G. Edwards, and C. Taylor, "Active Appearance Models," *Proc. European Conf. Computer Vision,* pp. 484-498, 1998.

[16] H. Jia and A.M. Martinez, "Face Recognition with Occlusions in the Training and Testing Sets," *Proc. IEEE Int'l Conf. Automatic Face and Gesture Recognition,* 2008.

[17] H. Jia and A.M. Martinez, "Support Vector Machines in Face Recognition with Occlusions," *Proc. IEEE Conf. Computer Vision and Pattern Recognition,* 2009.

[18] Z. Zhou, A. Wagner, H. Mobahi, J. Wright, and Y. Ma, "Face Recognition with Contiguous Occlusion Using Markov Random Fields," *Proc. IEEE Int'l Conf. Computer Vision,* 2009.

[19] K.-H. Jeonga, W. Liu, S. Han, E. Hasanbelliu, and J.C. Principe, "The Correntropy Mace Filter," *Pattern Recognition,* vol. 42, no. 5, pp. 871-885, 2009.

[20] J. Wright, Y. Ma, J. Mairal, G. Sapiro, T.S. Huang, and S. Yan, "Sparse Representation for Computer Vision and Pattern Recognition," *Proc. IEEE,* vol. 98, no. 6, pp. 1031-1044, 2010.

[21] E.J. Candes and T. Tao, "Decoding by Linear Programming," *IEEE Trans. Information Theory,* vol. 51, no. 12, Dec. 2005.

[22] D.L. Donoho, "For Most Large Underdetermined Systems of Linear Equations the Minimal L1-Norm Solution Is Also the Sparsest Solution," *Comm. Pure and Applied Math.,* vol. 59, no. 6, pp. 797-829, 2006.

[23] Y. Bengio, "Learning Deep Architectures for AI," *Proc. Foundations and Trends in Machine Learning,* 2009.

[24] J. Wright, A.Y. Yang, A. Ganesh, S.S. Sastry, and Y. Ma, "Robust Face Recognition via Sparse Representation," *IEEE Trans. Pattern Analysis and Machine Intelligence,* vol. 31, no. 2, pp. 210-227, Feb. 2009.

[25] X. He, S. Yan, Y. Hu, P. Niyogi, and H.-J. Zhang, "Face Recognition Using Laplacianfaces," *IEEE Trans. Pattern Analysis and Machine Intelligence,* vol. 27, no. 3, pp. 328-340, Mar. 2005.

[26] J. Wright and Y. Ma, "Dense Error Correction via L1-Minimization," *IEEE Trans. Information Theory,* vol. 54, no. 7, pp. 3035-3058, July 2008.

[27] W. Liu, P.P. Pokharel, and J.C. Principe, "Correntropy: Properties and Applications in Non-Gaussian Signal Processing," *IEEE Trans. Signal Processing,* vol. 55, no. 11, pp. 5286-5298, Nov. 2007.

[28] X. Yuan and B.-G. Hu, "Robust Feature Extraction via Information Theoretic Learning," *Proc. Int'l Conf. Machine Learning,* 2009.

[29] J.C. Principe, D. Xu, and J.W. Fisher, "Information-Theoretic Learning," *Unsupervised Adaptive Filtering, Volume 1: Blind-Source Separation,* S. Haykin, ed., Wiley, 2000.

[30] D. Xu, "Energy, Entropy, and Information Potential for Neural Computation," PhD dissertation, Univ. of Florida, 1999.

[31] T.M. Cover and J.A. Thomas, *Elements of Information Theory,* second ed. John Wiley, 2005.

[32] S.Z. Li and J. Lu, "Face Recognition Using Nearest Feature Line Method," *IEEE Trans. Neural Network,* vol. 10, no. 2, pp. 439-443, Mar. 1999.

[33] J. Laaksonen, "Local Subspace Classifier," *Proc. Int'l Conf. Artificial Neural Networks,* 1997.

[34] S.Z. Li, "Face Recognition Based on Nearest Linear Combinations," *Proc. IEEE Int'l Conf. Computer Vision and Pattern Recognition,* pp. 839-844, 1998.

[35] P. Vincent and Y. Bengio, "K-Local Hyperplane and Convex Distance Nearest Neighbor Algorithms," *Advances in Neural Information Processing Systems,* vol. 14, pp. 985-992, 2001.

[36] J.-T. Chien and C.-C. Wu, "Discriminant Wavelet Faces and Nearest Feature Classifiers for Face Recognition," *IEEE Trans. Pattern Analysis and Machine Intelligence,* vol. 24, no. 12, pp. 1644-1649, Dec. 2002.

[37] J. Ho, M.-H. Yang, J. Lim, K.-C. Lee, and D. Kriegman, "Clustering Appearances of Objects under Varying Illumination Conditions," *Proc. IEEE Int'l Conf. Computer Vision and Pattern Recognition,* vol. 1, pp. 11-18, 2003.

[38] P.P. Pokharel, W. Liu, and J.C. Principe, "A Low Complexity Robust Detector in Impulsive Noise," *Signal Processing,* vol. 89, no. 10, pp. 1902-1909, 2009.

[39] I. Santamaria, P.P. Pokharel, and J.C. Principe, "Generalized Correlation Function: Definition,Properties, and Application to Blind Equalization," *IEEE Trans. Signal Processing,* vol. 54, no. 6, pp. 2187-2197, June 2006.

[40] V. Vapnik, *The Nature of Statistical Learning Theory.* Springer-Verlag, 1995.
[41] W. Liu, P. Pokharel, and J. Principe, "Error Entropy, Correntropy and M-Estimation," *Proc. Workshop Machine Learning for Signal Processing,* 2006.
[42] P. Huber, *Robust Statistics.* Wiley, 1981.
[43] I. Mizera and C. Muller, "Breakdown Points of Cauchy Regression-Scale Estimators," *Statistics and Probability Letters,* vol. 57, no. 1, pp. 79-89, 2002.
[44] W. Yin, S. Osher, D. Goldfarb, and J. Darbon, "Bregman Iterative Algorithms for L1-Minimization with Applications to Compressed Sensing," *SIAM J. Imaging Sciences,* vol. 1, no. 1, pp. 143-168, 2008.
[45] S. Yang, H. Zha, S. Zhou, and B.-G. Hu, "Variational Graph Embedding for Globally and Locally Consistent Feature Extraction," *Proc. Europe Conf. Machine Learning,* pp. 538-553, 2009.
[46] S. Boyd and L. Vandenberghe, *Convex Optimization.* Cambridge Univ. Press, 2004.
[47] L.F. Portugal, J.J. Judice, and L.N. Vicente, "A Comparison of Block Pivoting and Interior-Point Algorithms for Linear Least Squares Problems with Non-Negative Variables," *Math. Computation,* vol. 63, no. 208, pp. 625-643, 1994.
[48] A.M. Martinez and R. Benavente, "The AR Face Database," technical report, Computer Vision Center, 1998.
[49] A.S. Georghiades, P.N. Belhumeur, and D.J. Kriegman, "From Few to Many: Illumination Cone Models for Face Recognition under Variable Lighting and Pose," *IEEE Trans. Pattern Analysis and Machine Intelligence,* vol. 23, no. 6, pp. 643-660, June 2001.
[50] P.J. Phillips, P.J. Flynn, T. Scruggs, K. Bowyer, J. Chang, K. Hoffman, J. Marques, J. Min, and W. Worek, "Overview of the Face Recognition Grand Challenge," *Proc. IEEE Conf. Computer Vision and Pattern Recognition,* 2005.
[51] K.-C. Lee, J. Ho, and D. Kriegman, "Acquiring Linear Subspaces for Face Recognition under Variable Lighting," *IEEE Trans. Pattern Analysis and Machine Intelligence,* vol. 27, no. 5, pp. 684-698, May 2005.
[52] H. Lee, A. Battle, R. Raina, and A.Y. Ng, "Efficient Sparse Coding Algorithms," *Proc. Int'l Conf. Advanced Neural Information Processing Systems,* 2006.
[53] E. Candes and J. Romberg L-Magic: Recovery of Sparse Signals via Convex Programming, http://www.acm.caltech.edu/l1magic/, 2005.
[54] E. Elhamifar and R. Vidal, "Sparse Subspace Clustering," *Proc. IEEE Conf. Computer Vision and Pattern Recognition,* pp. 2790-2797, 2009.
[55] D. Yi, R. Liu, R. Chu, Z. Lei, and S.Z. Li, "Face Matching from Near Infrared to Visual Images," *Proc. IAPR/IEEE Int'l Conf. Biometrics,* 2007.
[56] R. He, B.-G. Hu, and X. Yuan, "Robust Discriminant Analysis Based on Nonparametric Maximum Entropy," *Proc. Asian Conf. Machine Learning,* 2009.
[57] M. Nikolova and M.K. NG, "Analysis of Half-Quadratic Minimization Methods for Signal and Image Recovery," *SIAM J. Scientific Computing,* vol. 27, no. 3, pp. 937-966, 2005.
[58] K. Huang and S. Aviyente, "Sparse Representation for Signal Classification," *Proc. Int'l Conf. Advanced Neural Information Processing Systems,* 2006.
[59] G. Peyre, "Sparse Modeling of Textures," *J. Math. Imaging and Vision,* vol. 34, no. 1, pp. 17-31, 2009.

Ran He received the BS degree in computer science from the Dalian University of Technology of China and the PhD degree in pattern recognition and intelligent system from the Institute of Automation, Chinese Academy of Sciences, in 2009. He is currently an assistant professor with NLPR (National Laboratory of Pattern Recognition), Institute of Automation, Chinese Academy of Science, Beijing, China. His research interests include information theoretic learning and computer vision. He is a member of the IEEE Computer Society.

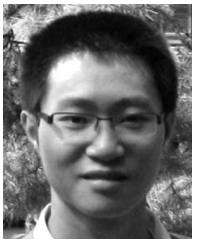

Wei-Shi Zheng received the PhD degree in applied mathematics from Sun Yat-Sen University, China, 2008. Since then, he has been a postdoctoral researcher on the European SAMURAI Research Project at the Department of Computer Science, Queen Mary University of London, United Kingdom. He joined Sun Yat-sen University under the one-hundred-people program in 2011. His current research interests are in object association and categorization for visual surveillance. He is also interested in discriminant/sparse feature extraction, dimension reduction, kernel methods in machine learning, transfer learning, and face image analysis. He is a member of the IEEE Computer Society.

Bao-Gang Hu received the MSc degree from the University of Science and Technology, Beijing, China, in 1983 and the PhD degree from McMaster University, Canada, in 1993, all in mechanical engineering. From 1994 to 1997, he was a research engineer and senior research engineer at C-CORE, Memorial University of Newfoundland, Canada. He is currently a professor with NLPR (National Laboratory of Pattern Recognition), Institute of Automation, Chinese Academy of Science, Beijing, China. From 2000 to 2005, he was the Chinese Director of LIAMA (the Chinese-French Joint Laboratory for Computer Science, Control, and Applied Mathematics). His main research interests include pattern recognition and plant growth modeling. He is a senior member of the IEEE and a member of the IEEE Computer Society.